JOURNAL OF COMPUTATIONAL PHYSICS **127,** 473–481 (1996)
ARTICLE NO. 0188

Implementation of an Electrostatic Implicit Particle Simulation Scheme

T. H. WATANABE, Y. TODO, R. HORIUCHI, K. WATANABE, AND T. SATO

Theory and Computer Simulation Center, National Institute for Fusion Science, Nagoya 464-01, Japan

Received May 8, 1995

We have developed an electrostatic macro-scale implicit particle simulation code which enables us to simulate low-frequency plasma wave phenomena with large spatial scale length. Specifically, the Poisson equation with the implicit susceptibility term is accurately solved in our scheme with the ''strict differencing'' and ''the consistent filtering.'' Linear properties of the simulation scheme, such as the linear stability and the dispersion relation, are examined. We have also applied our simulation code to the excitation and nonlinear saturation of the ion temperature gradient (ITG) drift instability in a system with a shearless slab geometry. The linear properties of the excited ITG mode are compared with the theoretical prediction to find a good agreement.

1. INTRODUCTION

In the last three decades, the particle simulation method has been employed for studying nonlinear plasma waves with kinetic effects such as the Landau and cyclotron dampings. While various nonlinear plasma phenomena have been clarified by the conventional particle simulation with explicit time integration, the applicability is limited to high-frequency plasma waves with short wavelengths. This is because the simulation time step Δt should be less than ω_p^{-1} and the grid spacing has to be comparable to the Debye length [1, 2]. Thus, it is difficult to study kinetic waves with MHD space and time scales by means of the conventional particle simulation method. In fusion and space plasmas, however, one notices the importance of kinetic effects on MHD and transport scale phenomena, such as the excitation of MHD waves by high energy (alpha) particles, anomalous heat transport caused by drift waves, triggering of collisionless reconnection and so on. For the purpose of obtaining a feasible tool that can be useful for the study of the nonlinear plasma dynamics with large space and time scales, many efforts have been made to overcome the technical restriction pertinent to the conventional particle simulation. The direct implicit particle simulation technique has been developed and improved by continuous efforts over the last decade [1–5]. In the direct method, particle data is directly used in the prediction of electromagnetic fields at the next time step. The essence of the direct method for an electrostatic model is to make prediction of charge density based on a linearized approximation, which depends only on particle positions, and to calculate the electrostatic potential at the next time step. In addition, an implicit equation of motion for each particle, which is numerically stable against the high-frequency plasma oscillation, is solved along with the Poisson equation which is modified with the implicit susceptibility term.

In the macro-scale particle simulation scheme [5], which is categorized in the direct implicit method, both the equation of motion and the Maxwell equation are solved by a first-order implicit algorithm. For electrostatic modes propagating along the magnetic field, however, no significant peak is recognizable in the power spectrum of the ion acoustic branch (see Fig. 6 in Ref. [5]). Therefore, for practical use an electrostatic macro-scale particle simulation scheme with low-noise level and high-accuracy is required to develop.

In order to improve the accuracy in calculation of the electrostatic field, some important methods have been proposed by the Livermore group [3, 6], that is, ''the consistent filtering'' and ''the strict differencing.'' The consistent filtering method has been applied to the electrostatic gravitational instability in the two-dimensional system [4]. Since the strict differencing scheme includes a difficulty in implementing a two- or three- dimensional scheme, no application with both the strict differencing and the consistent filtering has been made in multi-dimensions. Highly accurate solution of the implicit Poisson equation is, however, needed not only in ensuring simulation results, but also in guaranteeing the numerical stability of a simulation code. This is because the stability analysis of the code is practical and useful only when the solution of the Poisson equation is obtained accurately.

In this paper, we present an electrostatic version of the revised macro-scale particle simulation scheme and examine the validity of our method both analytically and numerically. A process of satisfying the implicit Poisson equation is necessary in the electromagnetic particle simulation in order to satisfy the charge continuity law. Thus, we wish to start with inventing an elaborate method of solving the

0021-9991/96 $18.00

implicit Poisson equation with high accuracy in this paper. The numerical algorithm will be described in Section 2. In Section 3, we will make stability analysis of our simulation scheme by means of the procedure given by Langdon [7], taking into account all the effects of the finite time step, the finite grid spacing, the alias modes, the shape function of particles, and the Maxwellian velocity distribution function. Our numerical technique for implementing the strict differencing in multi-dimensions is given in Section 4. Simulation results will be shown in Section 5, where the ion temperature gradient (ITG) drift instability will be examined by its two-dimensional version, including the effect of the polarization drift [8]. Summary and discussion will be given in the last section.

2. SIMULATION ALGORITHM

2.1. *Electrostatic Algorithm in 1D System*

At first let us consider an unmagnetized electrostatic plasma in a one-dimensional system. The equation of motion for each particle i with a shape function $S(x)$ is given by [5]

$$x_i^{n+1} = x_i^n + \Delta t v_i^n + \frac{q_i \Delta t^2}{2m_i} \sum_j \Delta x S(X_j - \bar{x}_i^{n+\alpha}) E_j^{n+\alpha}, \quad (1)$$

$$v_i^{n+1} = v_i^n + \frac{q_i \Delta t}{m_i} \sum_j \Delta x S(X_j - \bar{x}_i^{n+\alpha}) E_j^{n+\alpha}, \quad (2)$$

where x_i^n and v_i^n are a particle position and velocity at the nth time step; q_i and m_i denote the charge and mass of the particle; X_j means the position of a grid point and the suffix j indicates the grid number. The time-decentering parameter α is in the range of $0.5 \le \alpha \le 1$. When $\alpha = 0.5$, Eqs. (1) and (2) are time-centered. As is given in the above equations, the electric field $E^{n+\alpha}$, which is given by the linear interpolation of $E^{n+\alpha} = \alpha E^{n+1} + (1 - \alpha) E^n$, acts on the particle at $x = \bar{x}_i^{n+\alpha}$. Here, $\bar{x}_i^{n+\alpha}$ is provided by $\bar{x}_i^{n+\alpha} = x_i^n + \alpha \Delta t v_i^n$.

As is described in Eqs. (1) and (2), particles are accelerated by E^n and E^{n+1}, while E^{n+1} is unknown at the nth time step. In the implicit particle algorithm, thus, the Poisson equation is not solved directly, because the particle position x_i^{n+1}, hence, the charge density $\rho_j(x_i^{n+1})$ has not been obtained at the nth time step. Therefore, the Poisson equation at the $(n + 1)$th time step is approximated by the Taylor expansion at $\tilde{x}_i^{n+1}$,

$$-\nabla^2 \phi_j^{n+1} = \rho_j(x_i^{n+1})/\varepsilon_0 \quad (3)$$

$$\approx \rho_j(\tilde{x}_i^{n+1})/\varepsilon_0 + \delta\rho_j(\tilde{x}_i^{n+1})/\varepsilon_0 \quad (4)$$

with

$$\tilde{x}_i^{n+1} = x_i^n + \Delta t v_i^n + (1 - \alpha) \frac{q_i \Delta t^2}{2m_i} \sum_j \Delta x S(X_j - \bar{x}_i^{n+\alpha}) E_j^n. \quad (5)$$

Here,

$$\rho_j(\tilde{x}_i^{n+1}) = \sum_i q_i S(X_j - \tilde{x}_i^{n+1}) \quad (6)$$

and

$$\delta\rho_j(\tilde{x}_i^{n+1}) = -\nabla \cdot \sum_i \alpha \frac{q_i^2 \Delta t^2}{2m_i} \times S(X_j - \tilde{x}_i^{n+1}) \sum_l \Delta x S(X_l - \tilde{x}_i^{n+1})(-\nabla \phi_l^{n+1}). \quad (7)$$

After solving Eq. (4), one can calculate the particle position and velocity at the $(n + 1)$th time step. Conventionally, the implicit term in Eq. (7), which consists of spatial convolution, is further simplified [1, 3, 5] as

$$\delta\rho_j(\tilde{x}_i^{n+1}) \approx -\nabla \cdot \sum_i \alpha \frac{q_i^2 \Delta t^2}{2m_i} S(X_j - \tilde{x}_i^{n+1})(-\nabla \phi_j^{n+1}). \quad (8)$$

Note that the second summation of l in Eq. (7) is replaced by $-\nabla \phi_j^{n+1}$. This simplification (simplified differencing) reduces Eq. (4) to a tri- or penta-diagonal matrix equation of ϕ_j^{n+1}, if $S(x)$ is the *nearest-grid-point* or *linear-interpolation* function. In such a case, we can easily solve Eq. (4) by means of an adequate matrix equation solver.

The present study, however, has disclosed that the approximation in Eq. (8) results in a serious numerical error in association with the inconsistent filtering. Thus, Eq. (7) should be employed without any approximation and Eq. (4) should be solved iteratively. Numerical accuracy of our method will be examined in Section 5.1.

2.2. *Electrostatic Algorithm in 2D System*

In a two-dimensional case with an external magnetic field B, particle velocity perpendicular to the magnetic field is given by the E × B drift both for the electrons and ions. Only parallel velocity $\mathbf{v}_{\|i}^{n+1}$ is calculated from the equation of motion as

$$\mathbf{x}_i^{n+1} = \mathbf{x}_i^n + \Delta t \mathbf{v}_{\|i}^n + \sum_{j,k} \Delta x \Delta y S(\mathbf{X}_{jk} - \bar{\mathbf{x}}_i^{n+\alpha}) \times \left[\frac{\Delta t}{B^2} \mathbf{E}_{jk}^{n+\alpha} \times \mathbf{B} + \frac{q_i \Delta t^2}{2m_i} \mathbf{E}_{\|jk}^{n+\alpha} \right], \quad (9)$$

$$\mathbf{v}_{\|i}^{n+1} = \mathbf{v}_{\|i}^{n} + \frac{q_i \Delta t}{m_i} \sum_{j,k} \Delta x \Delta y S(\mathbf{X}_{jk} - \bar{\mathbf{x}}_i^{n+\alpha}) \mathbf{E}_{\|jk}^{n+\alpha}, \quad (10)$$

where $\bar{\mathbf{x}}_i^{n+\alpha} = \mathbf{x}_i^n + \alpha \Delta t \mathbf{v}_{\|i}^n$. The Poisson equation is modified by introducing the polarization term [8]:

$$-\nabla^2 \phi_{jk}^{n+1} - \nabla_\perp \cdot \frac{m_i n_0}{\varepsilon_0 B^2} \nabla_\perp \phi_{jk}^{n+1} = \rho_{jk}(\mathbf{x}_i^{n+1})/\varepsilon_0. \quad (11)$$

The above equation is also expanded at $\tilde{\mathbf{x}}_i^{n+1}$, where

$$\begin{aligned} \tilde{\mathbf{x}}_i^{n+1} &= \mathbf{x}_i^n + \Delta \mathbf{t} \mathbf{v}_{\|i}^n \\ &\quad + \sum_{j,k} \Delta x \Delta y S(\mathbf{X}_{jk} - \bar{\mathbf{x}}_i^{n+\alpha})(1-\alpha) \\ &\quad \times \left[\frac{\Delta t}{B^2} \mathbf{E}_{jk}^n \times B + \frac{q_i \Delta t^2}{2 m_i} \mathbf{E}_{\|jk}^n \right]. \end{aligned} \quad (12)$$

Then, we obtain the implicit Poisson equation in the two-dimensional system,

$$\begin{aligned} &-\nabla^2 \phi_{jk}^{n+1} - \nabla_\perp \cdot \frac{m_i n_0}{\varepsilon_0 B^2} \nabla_\perp \phi_{jk}^{n+1} \\ &\quad = \rho_{jk}(\tilde{\mathbf{x}}_i^{n+1})/\varepsilon_0 + \delta \rho_{jk}(\tilde{\mathbf{x}}_i^{n+1})/\varepsilon_0, \end{aligned} \quad (13)$$

with

$$\delta \rho_{jk}(\tilde{\mathbf{x}}_i^{n+1}) = -\nabla \cdot \sum_i q_i \delta \mathbf{x}_i S(\mathbf{X}_{jk} - \tilde{\mathbf{x}}_i^{n+1}). \quad (14)$$

The displacement vector $\delta \mathbf{x}_i$ for each particle is given by

$$\begin{aligned} \delta \mathbf{x}_i &= \sum_{l,m} \Delta x \Delta y S(\mathbf{X}_{lm} - \tilde{\mathbf{x}}_i^{n+1}) \alpha \\ &\quad \times \left[\Delta t \frac{-\nabla \phi_{lm}^{n+1} \times \mathbf{B}}{B^2} - \frac{q_i \Delta t^2}{2 m_i} \nabla_\| \phi_{lm}^{n+1} \right]. \end{aligned} \quad (15)$$

Solving Eqs. (9) and (10) with (13), we obtain the particle positions and velocities at the $(n+1)$th time step.

3. LINEAR ANALYSIS OF NUMERICAL STABILITY

In this section, we will investigate the numerical stability of our simulation scheme. According to the linear analysis given by Langdon [7], we will derive a dispersion relation in the model plasma for the one-dimensional case. Here, electron motions with respect to the background immobile ions are considered, because we are interested in stability against the plasma oscillation. Suppose a particle with an unperturbed trajectory of $x_{(0)}^{n+1} = x_{(0)}^0 + (n+1)\Delta t v_{(0)}$ is accelerated by a sinusoidal electric field $Ee^{ikX_j - i\omega(n+1)\Delta t}$. The perturbed particle position $x_{(1)}^{n+1}$ is expressed by the time integration of acceleration in the past, such as

$$\begin{aligned} x_{(1)}^{n+1} = \frac{q \Delta t^2}{m} \sum_{s=1} \Bigg\{ \left(s - \frac{1}{2} \right) \Delta x E [\alpha e^{-i\omega \Delta t} + (1-\alpha)] \\ e^{-i\omega(n+1-s)\Delta t} \sum_j e^{ikX_j} S(X_j - x_{(0)}^{n+1-s+\alpha}) \Bigg\}, \end{aligned} \quad (16)$$

where s is a positive integer. The first term in the square bracket at $s = 1$ corresponds to the implicit acceleration by E_j^{n+1}. Since the particle feels the electric field on its unperturbed trajectory in the linear regime, the argument of the shape function becomes $X_j - x_{(0)}^{n+1-s+\alpha}$. Taking average over all particles and operating the Fourier transformation, we obtain the dipole density $\mathscr{P}(k, n+1)$, which is separated into two parts:

$$\mathscr{P}(k, n+1) = -i[\mathscr{Q}(k) + \mathscr{R}(k)]\, \phi(k) e^{-i\omega(n+1)\Delta t}, \quad (17)$$

where

$$\begin{aligned} \mathscr{Q}(k) &= \omega_p^2 \Delta t^2 \kappa_E(k) S(k) \\ &\quad \times \Bigg\{ \sum_{s=2} \left(s - \frac{1}{2} \right) [\alpha e^{-i\omega \Delta t} + (1-\alpha)] e^{is\omega \Delta t} e^{-[k(s-\alpha)\Delta t]^2 v_t^2/2} \\ &\quad + \frac{1}{2}(1-\alpha) e^{i\omega \Delta t} e^{-[k(1-\alpha)\Delta t]^2 v_t^2/2} \Bigg\} \end{aligned} \quad (18)$$

$$\mathscr{R}(k) = \tfrac{1}{2} \omega_p^2 \Delta t^2 \kappa_E(k) S(k) \alpha e^{-[k(1-\alpha)\Delta t]^2 v_t^2/2}. \quad (19)$$

In the above equations, we have assumed the Maxwellian velocity distribution function, $f_0(v) = (1/\sqrt{2\pi} v_t) \exp(-v^2/2v_t^2)$. Moreover, $\kappa_E(k)$ means the finite difference gradient operator for calculating the electric field. It is worthwhile to note that the implicit term $\mathscr{R}(k)$ represents a plasma response to the electric field E^{n+1}, and that divergence of $-\mathscr{P}(k, n+1)$ gives the charge density ρ^{n+1}/ε_0. Substituting the divergence of Eq. (17) into the Fourier transformation of Eq. (4), we arrive at the dispersion relation of the implicit particle simulation plasma,

$$1 + \frac{1}{K^2(k)} \sum_p S(k_p)[k_p \mathscr{Q}(k_p) + \kappa_{\delta\rho}(k) \mathscr{R}(k_p)] = 0, \quad (20)$$

where $\kappa_{\delta\rho}(k)$ is the divergence operator for the implicit term in Eq. (7) and $K^2(k)$ means the Laplacian in the finite difference form. The index p shows the alias mode which arises in the calculation of the charge density defined on the spatial grids. Then, k_p is given by $k_p = k - p(2\pi/\Delta x)$. If the alias modes can be ignored, and if $\kappa_{\delta\rho}(k) = k$, we can simplify the dispersion relation of Eq. (20) as

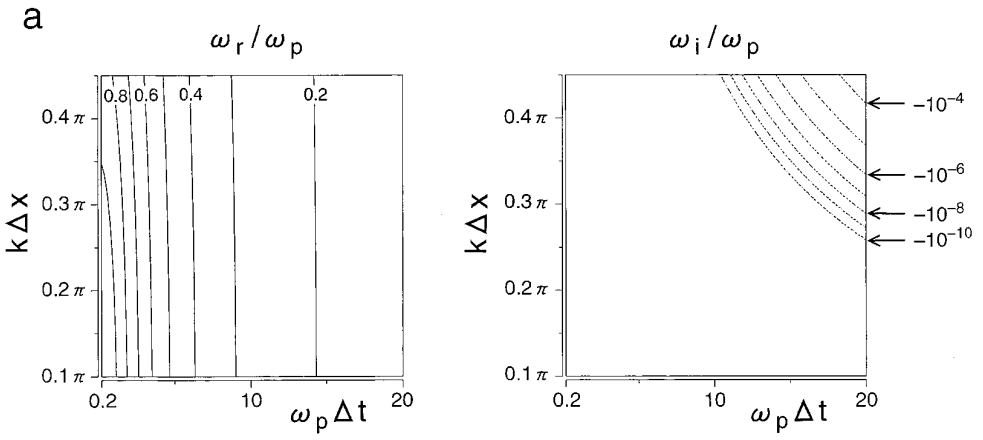

FIG. 1. Numerical solutions of the dispersion relation obtained from the linear analysis of the simulation scheme for the cases of (a) $\alpha = 0.5$ without the alias modes, (b) $\alpha = 0.5$, and (c) $\alpha = 0.55$ with the alias modes. Solid and dashed contour lines indicate positive and negative values, respectively. For the real part of the solutions (left), the contour interval of ω_r/ω_p is 0.1 in all cases of (a)–(c). For the imaginary part (right), the contour levels in case (a) are logarithmically defined as -10^{-10}, -10^{-9}, ..., -10^{-4}; in cases (b) and (c), the contour interval of ω_i/ω_p is equal to 4×10^{-3}.

$$1 + \frac{\omega_p^2 \Delta t^2}{K^2(k)} k\kappa_E(k) S^2(k) \times \sum_{s=1} \left(s - \frac{1}{2}\right) [\alpha e^{-i\omega\Delta t} + (1-\alpha)] e^{is\omega\Delta t} e^{-[k(s-\alpha)\Delta t]^2 v_t^2/2} = 0. \tag{21}$$

In remainder of this section, we numerically solve Eqs. (20) and (21) in a frequency domain of the plasma oscillation and examine the numerical stability of our simulation method.

First, let us consider a case without the aliasing effect ($p = 0$), calculating real and imaginary parts of ω (i.e., ω_r and ω_i) in Eq. (21) by the Newton method. In our actual simulation code, we have used the following operators:

$$K^2(k) = k^2 \left[\frac{\sin(k\Delta x/2)}{k\Delta x/2}\right]^2 \tag{22}$$

$$\kappa_E(k) = k \left[\frac{\sin(k\Delta x)}{k\Delta x}\right] \tag{23}$$

$$\kappa_{\delta p}(k) = k. \tag{24}$$

We take the divergence of Eq. (7) in the wavenumber space so that Eq. (24) is satisfied. Hence, Eq. (21) is valid when the alias modes are dismissed. The shape function which we have employed is the *linear-interpolation* function,

$$S(k) = \left[\frac{\sin(k\Delta x/2)}{k\Delta x/2}\right]^2. \tag{25}$$

Numerical solutions of Eq. (21) with parameters of $\Delta x = 12.5\pi\lambda_D$ and $\alpha = 0.5$ are shown in Fig. 1a, where contours of ω_r and ω_i are plotted in $\Delta t - k$ plane; ω_r decreases as Δt and k increase, respectively, because of the implicit time-difference and the finite grid effect. The minimum frequency in the $\Delta t - k$ plane is $\omega_r = 0.147\omega_p$. More importantly, ω_i has a small negative value for $\omega_p\Delta t \gg 1$. Our implicit scheme is, thus, numerically stable, when the alias modes are ignored.

Secondly, we solve Eq. (20) under the same numerical parameters and operators as in the case of Fig. 1(a). Here, the aliasing effect ($p \neq 0$) is fully taken into account. The numerical result is given in Fig. 1(b). One can see that the decrement of ω_r against k is larger than that of the case shown in Fig. 1(a). Undesirably, there are unstable solutions (positive ω_i) due to the aliasing effect in a wide range of the wavenumber space. The numerical instability caused by the alias modes can be stabilized, if we use a much smaller grid spacing such as $\Delta x \sim \lambda_D$. In order to realize a particle simulation with an MHD spatial scale, however, it is necessary to take a large grid spacing ($\Delta x \gg \lambda_D$). Although the employment of a higher order (much smoother) shape function is a candidate to suppress the numerical instability, it makes the simulation code much more complicated. Thus, we will introduce a stabilizing effect of the time-decentered scheme, increasing the decentering parameter α.

We have plotted solutions of Eq. (20) with $\alpha = 0.55$ in Fig. 1(c). While ω_r is quite similar to the case in Fig. 1(b), ω_i in $\Delta t - k$ space is largely modified by the time-decentering effect. The unstable solution, $\omega_i > 0$, is confined in a large wavenumber region, $k\Delta x > 0.3\pi$. No unstable solution is found in a small wavenumber region, $k\Delta x < 0.3\pi$, even in the case of $\omega_p\Delta t \gg 1$. If we further introduce an adequate numerical filter which can damp the large wavenumber

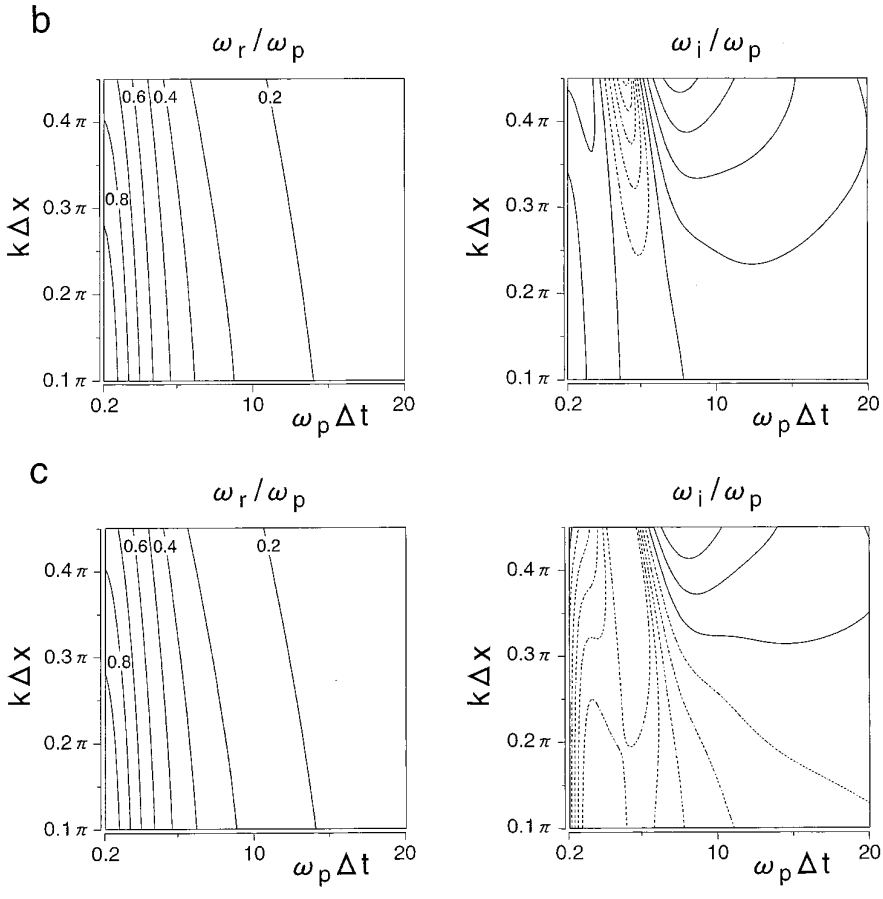

FIG. 1—*Continued*

mode of $k\Delta x > 0.3\pi$, we can realize a stable simulation code against the large time step ($\omega_p\Delta t \gg 1$) and the large grid spacing ($\Delta x \gg \lambda_D$). Therefore, we will use a numerical filter defined by [1]

$$W(k) = \exp[-(k/k_c)^{N_f}]. \tag{26}$$

Here, the cutoff wavenumber of $k_c = 2\pi/8\Delta x$ is sufficient for our purpose. The integer N_f, which is set to be 4 or 8 in the later simulations, controls the sharpness of the numerical filter. In addition, the numerical filter should be employed both for $\rho(\tilde{x}_i^{n+1})$ and $\delta\rho(\tilde{x}_i^{n+1})$ consistently [3, 5]. Otherwise, usage of the numerical filter will degrade the accuracy of the electrostatic field calculation.

4. STRICT TREATMENT OF THE IMPLICIT TERM

In obtaining the future electrostatic potential ϕ^{n+1} in an implicit particle simulation, the implicit Poisson equation such as Eq. (4) is employed. After having solved the implicit equation, particles are pushed by the electric field E^{n+1} ($=-\nabla\phi^{n+1}$). Hence, it is not guaranteed that the future charge density $\rho(x_i^{n+1})$ and ϕ^{n+1} satisfy the Poisson equation, that is, Eq. (3). Before going into a real simulation, therefore, we must examine how the numerical error due to the implicit term $\delta\rho$ arises and how large it is. Numerical error arising from treatment of the implicit term has been investigated by the Livermore group [3, 6]. They found that the consistent filtering and the strict differencing largely improved the solution of the implicit Poisson equation. Hence, our subject is how to implement the multi-dimensional simulation scheme with strict treatment of the implicit term.

In some of previous works [3, 5, 6], the implicit term was moved to the left-hand side; hence, Eq. (4) was rewritten in a matrix form,

$$M_{jk}\phi_k^{n+1} = \rho_j(\tilde{x}_i^{n+1}). \tag{27}$$

When Eq. (27) is solved in real space, it is difficult to operate the numerical filter on the implicit term and to employ the strict differencing, especially in multi-dimensions. This is because the filter should be transformed into

real space in terms of a convolution operator which will, generally, lead to a large number of non-zero elements of M_{jk}. In order to use the consistent filtering, Barnes *et al.* [4] solved the implicit Poisson's equation in wavenumber space, while simplified differencing was employed.

In our simulation scheme, Eq. (4) is solved iteratively by means of the Newton–Raphson method, leaving the implicit term on the right-hand side. Thus, we can introduce strict differencing in the multi-dimensional system. We rewrite Eq. (4) as

$$-\nabla^2\phi_j = \rho_j(\tilde{x}_i)/\varepsilon_0 - \frac{\alpha\Delta t^2}{2} W^2 * \nabla \cdot N_{jl}E_l \tag{28}$$

with

$$N_{jl} = \sum_l \sum_i \frac{q_i^2}{m_i} S(X_j - \tilde{x}_i)\Delta x S(X_l - \tilde{x}_i) \tag{29}$$

and

$$E_l = -\nabla\phi_l, \tag{30}$$

where the superscript $n+1$ is neglected and W^2* denotes the filtering operation. For the *linear-interpolation* function $S(x)$, the matrix N_{jl} couples E_l at nine grid points in two dimensions and couples E_l at 27 grid points in three dimensions. It is important to note that the number of elements in N_{jl} is *not* changed by the filtering, while the number of elements in M_{jk} in Eq. (27) is largely increased. Furthermore, N_{jl} is fixed through the iteration steps; in other words, the particle data is referred to only at $(m) = 0$. Then, we solve Eq. (28) iteratively adding a dummy term on both sides of the equation, that is,

$$\begin{aligned} -\nabla^2\psi_j^{(m+1)} + \frac{\alpha\Delta t^2}{2}\nabla \cdot n_j(-\nabla\psi_j^{(m+1)}) \\ = \rho_j(\tilde{x}_i)/\varepsilon_0 - \frac{\alpha\Delta t^2}{2} W^2 * \nabla \cdot N_{jl}E_l^{(m)} \\ + \frac{\alpha\Delta t^2}{2}\nabla \cdot n_j(-\nabla\phi_j^{(m)}) \end{aligned} \tag{31}$$

and

$$\phi_j^{(m+1)} = \beta\psi_j^{(m+1)} + (1-\beta)\phi_j^{(m)}. \tag{32}$$

Here, (m) means the iteration step, and n_j is given by

$$n_j = W^2 * \sum_i \frac{q_i^2}{m_i} S(X_j - \tilde{x}_i). \tag{33}$$

The dummy term, which is the same with the simplified implicit term, is needed for accelerating the convergence of solution with long wave length. Moreover, Eq. (31) can be easily written in a matrix form for $\psi_j^{(m+1)}$ and, then, is solved by a matrix solver such as the conjugate-gradient method. Starting from the initial guess of $\phi_l^{(0)} = 0$, we have succeeded in finding the solution of Eq. (4), although the convergence of the iteration in Eqs. (31) and (32) may not be guaranteed for all spatial distributions of particles. Actually, in two-dimensional simulations shown in Section 5.3, we set $\beta = 0.5$. Then the solution is obtained after about 50 steps of iteration with the residual less than 10^{-8}. Through one-dimensional simulation runs in the next section, we examine the accuracy of our code with both the strict differencing and the consistent filtering.

5. SIMULATION RESULTS

5.1. *Numerical Accuracy in Electrostatic Field Calculation*

Giving an initial density perturbation of $\delta n \propto \sin(kx)$ for both the elecrons and ions, we have performed several one-dimensional simulations for varying wavenumbers over a hundred time steps with the periodic boundary condition. Parameters used in the simulations are as follows: $\alpha = 0.55$, $L_x = 128\Delta x$, $\Delta x = 12.5\pi\lambda_D$, $\Delta t = 10\omega_p^{-1}$, $m_i = 100m_e$, and $T_i = 0.01T_e$, where L_x means the system length; m_i, m_e, T_i, and T_e denote the masses and the temperatures of the ions and electrons. We have employed 1024 particles per grid spacing both for the electrons and the ions. The averaged value of δ, which is defined as

$$\delta \equiv \frac{\varepsilon_0 K^2(k)\phi^{n+1}(k)}{\rho^{n+1}(k)}, \tag{34}$$

over a hundred time steps is plotted as a function of the wavenumber in Fig. 2, where the white and black circles, respectively, represent the results for the cases with strict and simplified implicit terms. The dashed line indicates the analytical estimation with the simplified differencing and the inconsistent filtering given by

$$\delta \approx \frac{1}{1 + (\alpha/2)\omega_p^2\Delta t^2(1 - S^2(k)W^2(k))}. \tag{35}$$

In the case of the strict implicit term, the values of δ are irrespective of k and nearly equal to 1. The numerical error is less than 5%. Employing the strict expression of the implicit term in Eq. (7), therefore, we can perform a simulation run with high numerical accuracy for the potential calculation. In the simplified case, however, the value of δ monotonically decreases as k increases, as the analytical prediction, i.e., Eq. (35), gives. The large difference between $\varepsilon_0 K^2(k)\phi^{n+1}(k)$ and $\rho^{n+1}(k)$ arises for a much smaller

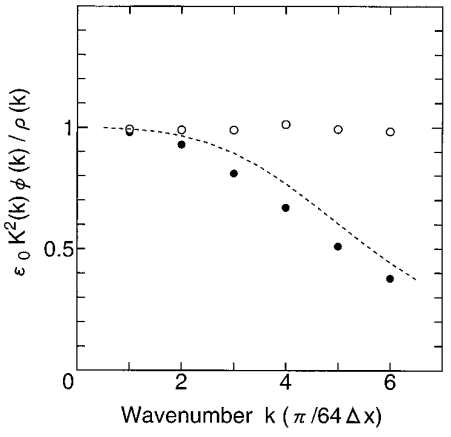

FIG. 2. Plots of the electrostatic fields obtained from the actual simulation runs with the strict (white circles) and simplified (black circles) implicit terms. Dashed line shows the theoretical estimation given by Eq. (35), where both the simplification of the implicit term and the inconsistent filtering are employed.

wavenumber regime than the cutoff wavenumber k_c ($=2\pi/8\Delta x$); for example, the error reaches 60% of $\rho^{n+1}(k)$ at $k = 6\pi/64\Delta x$.

5.2. *The Dispersion Relation of Electrostatic Waves*

Employing the strict implicit term given in Eq. (7), we have performed the simulation runs for the same parameters with those in the last subsection. In the present simulations, 8192 particles per grid spacing are used. We have obtained the dispersion relation of the electrostatic waves after having run the simulation code over 8192 time steps. Throughout the simulation run, the total energy in the simulation system is conserved within an error of 1%.

The power spectra of the electrostatic potential in the $\omega - k$ plane are plotted in Fig. 3. The dashed curve represents the dispersion relation of the ion acoustic wave, that is, $\omega = kC_s$ ($C_s = \sqrt{T_e/m_i}$). In low frequency regime ($\omega \approx 10^{-4}$–$10^{-3}\omega_p$), one can find the significant peaks which are coincident with the theoretical dispersion relation of the ion acoustic mode. The plasma oscillation, of which the frequency ($\omega_{pm} \simeq 0.27\omega_p$) is modulated by the implicit time-difference, can also be detected in the power spectra. The observed frequencies for the above two modes are in good agreement with the theoretical values.

In the power spectra, we have found two artificial modes. One of them, which may be generated by the numerical error in Eq. (4), is seen at the Nyquist frequency $\omega_N = \pi/\Delta t$. The other mode in an intermediate frequency range of $\omega \sim 10^{-2}$–$10^{-1}\omega_p$ would be caused by the mode coupling of ω_{pm} and ω_N. This is because the frequency spectra with band width of $0.06\omega_p$ are centered around $\omega_N - \omega_{pm}$ and the band width is similar to that of the frequency-modulated plasma oscillation. Moreover, we have confirmed that the power spectra of the artificial modes are independent of the ion to electron mass ratio. The artificial modes, thus, will not affect the low-frequency wave dynamics where the dynamics of ions plays the leading role.

5.3. *Simulation of the ITG Drift Instability*

We have performed two-dimensional simulations of the ITG drift instability in a system with a shearless slab geometry for several different time steps. The simulation system is set in the x-y plane. External magnetic field in the y-z plane is imposed on the system with an inclination angle of $\theta = \tan^{-1}(k_\parallel/k_\perp)$, where $\theta = 0.01$ in the present simulations. The electrostatic potential is fixed to zero at $x = 0$ and L_x, while the periodic boundary condition is employed in the y direction. The ion temperature profile in the x direction is given by

$$T_i(x) = T_{i0}\kappa_T L_x \frac{\exp(-\kappa_T x)}{1 - \exp(-\kappa_T L_x)}, \tag{36}$$

where $\kappa_T = 1.6 \times 10^{-3}\lambda_D^{-1}$ and $T_{i0} = T_e$. Other parameters are set as follows: the system length, $L_x = L_y = 16\Delta$; the grid spacing, $\Delta = \Delta x = \Delta y$; the ion to electron mass ratio, $m_i/m_e = 1836$; and number of particles per unit cell, $N\Delta = 1024$. The magnetic field intensity is determined so that $\Omega_e = \omega_p$, where Ω_e is the electron cyclotron frequency. In the two-dimensional case with the inclined magnetic field and the polarization term, the critical time step Δt_c for the explicit time integration is governed by the electrostatic shear Alfvén frequency [8] $\omega_H = (k_\parallel/k_\perp)(m_e/m_i)^{1/2}\Omega_e$; i.e., $\Delta t_c = \omega_H^{-1} = 4285\omega_p^{-1}$ for the present parameters. Thus, we will show that our implicit scheme is numerically stable for the time step Δt larger than Δt_c, while the explicit scheme is unstable in the case of $\Delta t > \Delta t_c$. We have carried out five simulation runs, changing the time step ($\Delta t =$

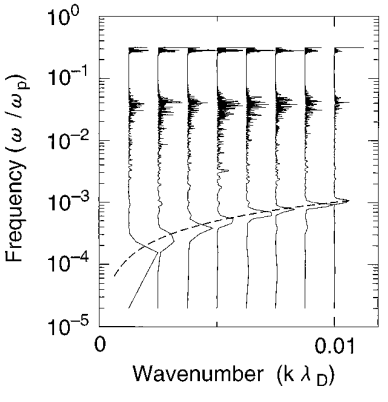

FIG. 3. Power spectra of the electrostatic potential obtained from the one-dimensional simulation. Dashed curve represents the theoretical dispersion relation of the ion acoustic mode.

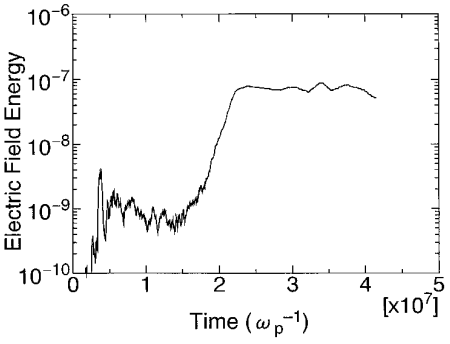

FIG. 4. Time evolution of the electric field energy for the two-dimensional simulation of the ITG drift instability. In this case, the simulation time step is set to be $1 \times 10^4 \omega_p^{-1}$. The growth rate of the instability obtained by the simulation is consistent with the theoretical value based on the fluid approximation.

2.5×10^3–$3 \times 10^4 \omega_p^{-1}$). In the following simulations, only the ITG mode with wavelength of L_y can be excited, because shorter wavelength modes ($k \geq k_c = 2\pi/8\Delta$) are artificially damped by the numerical filter for stabilization of the scheme.

Time evolution of the electric field energy is shown in Fig. 4. Here, $\Delta = 62.5\pi\lambda_D$ and $\Delta t = 1 \times 10^4 \omega_p^{-1}$. The field energy exponentially increases with the growth rate of $4.0 \times 10^{-7}\omega_p$ as the ITG drift instability is generated. Using the maximum entropy method, we have calculated the real frequency to obtain $\omega_r = 6 \times 10^{-7}\omega_p$. The frequency and growth rate obtained from the simulation are in fairly good agreement with the theoretical estimate given by the well-known dispersion relation under the fluid approximation [9],

$$\omega = \left(\frac{1}{2} + i\frac{\sqrt{3}}{2}\right)\left(\frac{k_\parallel^2 C_s^2}{2}\omega_{Ti}^*\right)^{1/3}. \tag{37}$$

For the present parameters, $\omega = 3.5 \times 10^{-7} + i6.0 \times 10^{-7}\omega_p$. The instability saturates at $t = 2.2 \times 10^7 \omega_p^{-1}$. The saturation level of the field energy is about $10^{-7} nT_e$. In Table I, the growth rates of the instability are summarized for the cases of $\Delta t = 0.25$, 0.5, 1.0, 2.0, and $3.0 \times 10^4 \omega_p^{-1}$.

TABLE I

Growth Rates of the ITG Drift Instability for Different Time Steps

Time step (ω_p^{-1})	Growth rate (ω_p)
2.5×10^3	4.9×10^{-7}
5.0×10^3	4.9×10^{-7}
1.0×10^4	4.0×10^{-7}
2.0×10^4	2.8×10^{-7}
3.0×10^4	3.9×10^{-7}

As is seen in Table I, the growth rate fluctuates in the large Δt regime owing to the numerical error. Nonetheless, all sautration levels of the field energy for the five cases are nearly equal to $10^{-7} nT_e$. Therefore, our implicit scheme is said to be stable even if $\Delta t > \Delta t_c$, and is applicable to a real low frequency phenomenon such as the ITG drift instability.

6. SUMMARY AND DISCUSSION

In the present study, we have developed an electrostatic version of the macro-scale implicit particle simulation code (MACS-ES) and have examined its characteristics analytically and numerically. The results are summarized as follows:

1. We have derived the linear dispersion relation of our new implicit particle simulation scheme and have verified its stability by solving the dispersion relation numerically. The linear analysis has shown that the unstable solutions due to the aliasing effect exist in the wide wavenumber regime for the time-centered difference scheme. In order to suppress the numerical instability, we have introduced the stabilizing effect of the time-decentered scheme and have employed the numerical filter leading to the damping of large wavenumber modes.

2. The numerical method for solving the implicit Poisson's equation has been improved in this study. Both of the strict differencing and the consistent filtering are employed in one- and two-dimensional systems. The accuracy of the electrostatic field calculation, thus, becomes much improved. The improvement is verified by the actual simulations.

3. The dispersion relations of electrostatic waves have been examined by means of the one-dimensional simulation. The power spectra in the ω-k space have shown good coincidence with the theoretical dispersion relation. Especially, the ion acoustic branch is clearly identified in the ω-k diagram.

4. Based on the scheme developed in one-dimensional case, we have extended our code to the two-dimensional geometry with the external magnetic field. In the two-dimensional model, the effect of the polarization drift is taken into account. Giving the ion temperature gradient perpendicular to the magnetic field, we have carried out simulations of the ITG drift instability. The obtained frequency and growth rate of the ITG mode are in reasonably good agreement with theoretically predicted ones. The growth rate of the instability, however, is found to fluctuate in a certain range when the time step Δt is changed as shown in Table I.

For stabilization of the alias modes, the high-frequency waves, such as the plasma oscillation in the one-dimen-

sional case and the electrostatic shear Alfvén wave in the two-dimensional case, are artificially attenuated in our scheme. Strictly speaking, the total energy in the implicit particle simulation plasma is not conserved, since the artificial damping of plasma waves causes numerical cooling of particles as is pointed out in previous works [3, 10, 11]. For example, the total energy in the two-dimensional simulations in Section 5.3 fluctuates within a level of 0.5% of the initial value. The energy conservation rate observed in the simulation is not sufficient for our purpose, when we intend to simulate a weakly saturated instability such as the ITG drift instability. Additionally, the numerical cooling may result in the fluctuation of the growth rate seen in Table I. In order to reduce the excessive cooling, it is important to suppress the numerical noise associated with the high-frequency waves. In addition to employing a higher order algorithm [10], the δf method [12–14] is one potential candidate which can decrease the numerical noise resulting from the finite number of particles. Since the δf method is designed for an explicit time integration, however, an implicit δf method [15] needs to be implemented.

ACKNOWLEDGMENTS

Numerical computations in this study are performed on the NIFS Advanced Computing System for Complexity Simulation. One of the authors (T.H.W.) is grateful to Dr. H. Naitou for fruitful discussions. This work is partially supported by Grants-in-Aid of the Ministry of Education, Science and Culture (No. 05836038 and No. 06044238).

REFERENCES

1. C. K. Birdsall and A. B. Langdon, *Plasma Physics via Computer Simulation* (McGraw–Hill, New York, 1985).
2. T. Tajima, *Computational Plasma Physics: With Applications to Fusion and Astrophysics* (Addison–Wesley, New York, 1989).
3. A. B. Langdon, B. I. Cohen, and A. Friedman, *J. Comput. Phys.* **51,** 107 (1983).
4. D. C. Barnes, T. Kamimura, J.-N. Leboeuf, and T. Tajima, *J. Comput. Phys.* **52,** 480 (1983).
5. M. Tanaka, *J. Comput. Phys.* **79,** 209 (1988).
6. B. I. Cohen, A. B. Langdon, and A. Friedman, *J. Comput. Phys.* **56,** 51 (1984).
7. A. B. Langdon, *J. Comput. Phys.* **30,** 202 (1979).
8. W. W. Lee, *J. Comput. Phys.* **72,** 243 (1987).
9. L. I. Rudakov and R. Z. Sagdeev, *Sov. Phys.-Dokl.* **6,** 415 (1961).
10. B. I. Cohen, A. B. Langdon, and A. Friedman, *J. Comput. Phys.* **46,** 15 (1982).
11. B. I. Cohen, A. B. Langdon, Hewett, and Procassini, *J. Comput. Phys.* **81,** 151 (1989).
12. M. Kotschenreuther, *Bull. Am. Phys. Soc.* **33,** 2107 (1988).
13. A. M. Dimits and W. W. Lee, *J. Comput. Phys.* **107,** 309 (1993).
14. S. E. Parker and W. W. Lee, *Phys. Fluids B* **5,** 77 (1993).
15. D. C. Barnes, *Bull. Am. Phys. Soc.* **36,** 1794 (1991).